



HAL
open science

Water Production in Comets C/2011 l4 (PanSTARRS) and C/2012 f6 (Lemmon) from observations with SOHO/SWAN

M. R. Combi, Jean-Loup Bertaux, Eric Quémerais, Stéphane Ferron, J. T. T.
Mäkinen, G. Apteekar

► To cite this version:

M. R. Combi, Jean-Loup Bertaux, Eric Quémerais, Stéphane Ferron, J. T. T. Mäkinen, et al.. Water Production in Comets C/2011 l4 (PanSTARRS) and C/2012 f6 (Lemmon) from observations with SOHO/SWAN. *The Astronomical Journal*, 2014, 147 (6), 126 (7 pp.). 10.1088/0004-6256/147/6/126 . hal-00988422

HAL Id: hal-00988422

<https://hal.science/hal-00988422v1>

Submitted on 18 Jul 2020

HAL is a multi-disciplinary open access archive for the deposit and dissemination of scientific research documents, whether they are published or not. The documents may come from teaching and research institutions in France or abroad, or from public or private research centers.

L'archive ouverte pluridisciplinaire **HAL**, est destinée au dépôt et à la diffusion de documents scientifiques de niveau recherche, publiés ou non, émanant des établissements d'enseignement et de recherche français ou étrangers, des laboratoires publics ou privés.

WATER PRODUCTION IN COMETS C/2011 L4 (PanSTARRS) AND C/2012 F6 (LEMMON) FROM OBSERVATIONS WITH *SOHO*/SWAN

M. R. COMBI¹, J.-L. BERTAUX², E. QUÉMERAIS², S. FERRON³, J. T. T. MÄKINEN⁴, AND G. APTEKAR¹

¹Department of Atmospheric, Oceanic and Space Sciences, University of Michigan, 2455 Hayward Street, Ann Arbor, MI 48109-2143, USA; mcombi@umich.edu

²LATMOS/IPSL, Université de Versailles Saint-Quentin 11, Boulevard d'Alembert, F-78280 Guyancourt, France
³ACRI-st, F-06904 Sophia-Antipolis, France

⁴Finnish Meteorological Institute, P.O. Box 503, FI-00101 Helsinki, Finland
Received 2013 November 8; accepted 2014 March 3; published 2014 April 24

ABSTRACT

Comets C/2011 L4 (PanSTARRS) and C/2012 F6 (Lemmon) were observed throughout their 2012–2013 apparitions with the Solar Wind Anisotropies (SWAN) all-sky hydrogen Ly α camera on board the *Solar and Heliosphere Observatory* (*SOHO*) satellite. *SOHO* has been in a halo orbit around the L1 Earth–Sun Lagrange point since early 1996 and has been observing the interplanetary medium and comets beginning with C/1996 B2 (Hyakutake). The global water production from these comets was determined from an analysis of the SWAN Ly α camera observations. Comet C/2011 L4 (PanSTARRS), which reached its perihelion distance of 0.302 AU on 2013 March 10.17, was observed on 50 days between 2013 January 29 and April 30. Comet C/2012 F6 (Lemmon), which reached its perihelion distance of 0.731 AU on 2013 March 24.51, was observed on 109 days between 2012 November 29 and 2013 June 31. The maximum water production rates were $\sim 1 \times 10^{30}$ molecules s⁻¹ for both comets. The activities of both comets were asymmetric about perihelion. C/2011 L4 (PanSTARRS) was more active before perihelion than after, but C/2012 F6 (Lemmon) was more active after perihelion than before.

Key words: comets: general – comets: individual (2011 L4 (PanSTARRS), 2012 F6 (Lemmon)) – ultraviolet: general

1. INTRODUCTION

Comet C/2011 L4 (PanSTARRS) was discovered by Richard Wainscoat with the Pan-STARRS 1 survey telescope on 2011 June 6 (Wainscoat et al. 2011). The comet's orbit has an inclination of 84°208 and, given its original semi-major axis, would be classified as a true Oort Cloud comet, indicating that it is most likely on its first trip back into the inner solar system since it was formed approximately 4.5 Gyr ago. Comet C/2012 F6 (Lemmon) was discovered on 2012 March 23 by Alex Gibbs with the Mt. Lemmon Survey telescope (Gibbs 2012). The comet's orbit has an inclination of 82°608, and unlike C/2011 L4, it definitely has an eccentricity less than one, indicating a semi-major axis of ~ 490 AU and that it is a long-period comet that has likely been through the inner solar system in the past. (Cometary ephemerides and orbital elements were obtained from the JPL Horizons Web site <http://ssd.jpl.nasa.gov/horizons.cgi>.)

At this time there is not yet much observational information available about either comet. Paganini et al. (2013), in an IAU Circular, reported infrared spectroscopic observations of C/2012 F6 (Lemmon) on 2013 March 31 and April 1. They found water production rates of 4.8 and 6.6×10^{29} s⁻¹ on those dates, respectively. They also report relative production rates of several other volatile species. They find that 2012 F6 is somewhat depleted in C₂H₆ and CH₃OH compared to the averages for Oort Cloud and long-period comets, with H₂CO slightly enhanced and CO and CH₄ average. All these ratios are in the normal spread of ranges of relative composition for typical comets with no remarkable deviations.

We report here on the results of analyses of observations of both of these comets made with the Solar Wind Anisotropies (SWAN) instrument on the *Solar and Heliospheric Observatory* (*SOHO*) spacecraft. *SOHO* has been in a halo orbit around the L1

Lagrange point, about 1 million km sunward of the Earth, since early 1996. The SWAN instrument was included on *SOHO*, a solar observatory, to study the global three-dimensional structure of the solar wind. The solar wind streaming out from the Sun encounters and ionizes the neutral interstellar hydrogen wind streaming into the solar system from the interplanetary medium (IPM) and carves out a pattern in the full-sky image that changes with the level of solar activity. SWAN consists of a scanning Ly α imager with two sensors, one accessing the north ecliptic hemisphere of the sky and the other accessing the south. Each one has a $5^\circ \times 5^\circ$ field of view (FOV) with $1^\circ \times 1^\circ$ pixels. In so-called full-sky mode, SWAN maps the entire sky in about one day.

The spatially expansive atomic hydrogen coma comes predominantly ($\sim 96\%$) both directly from the photodissociation of water as well as from the photodissociation of OH, which itself is produced in the main branch of water dissociation. As such, water production rates can be determined quite accurately from the analysis of observations of hydrogen in comets. Orbiting the L1 Lagrange point far from Earth and with access to the full-sky, *SOHO* avoids many of the temporal and sky location limits of ground-based observations of comets, such as high air mass and bright sky twilight observations, and northern/southern hemisphere limitations. SWAN also has a smaller solar avoidance area around the Sun, so it does not have some of the limitations of low Earth orbit-based observations.

SWAN has not made special targeted observations since the *Rosetta* mission targeted comet 67P/Churyumov–Gerasimenko in 2009 (Bertaux et al. 2014). However, SWAN continues to make full-sky observations every day so that it can obtain useful images of all comets that are bright enough throughout a large portion of their apparitions. Therefore, the full-sky observations are still very useful for determining water production rates in many comets with levels larger than about a few $\times 10^{27}$ s⁻¹ and

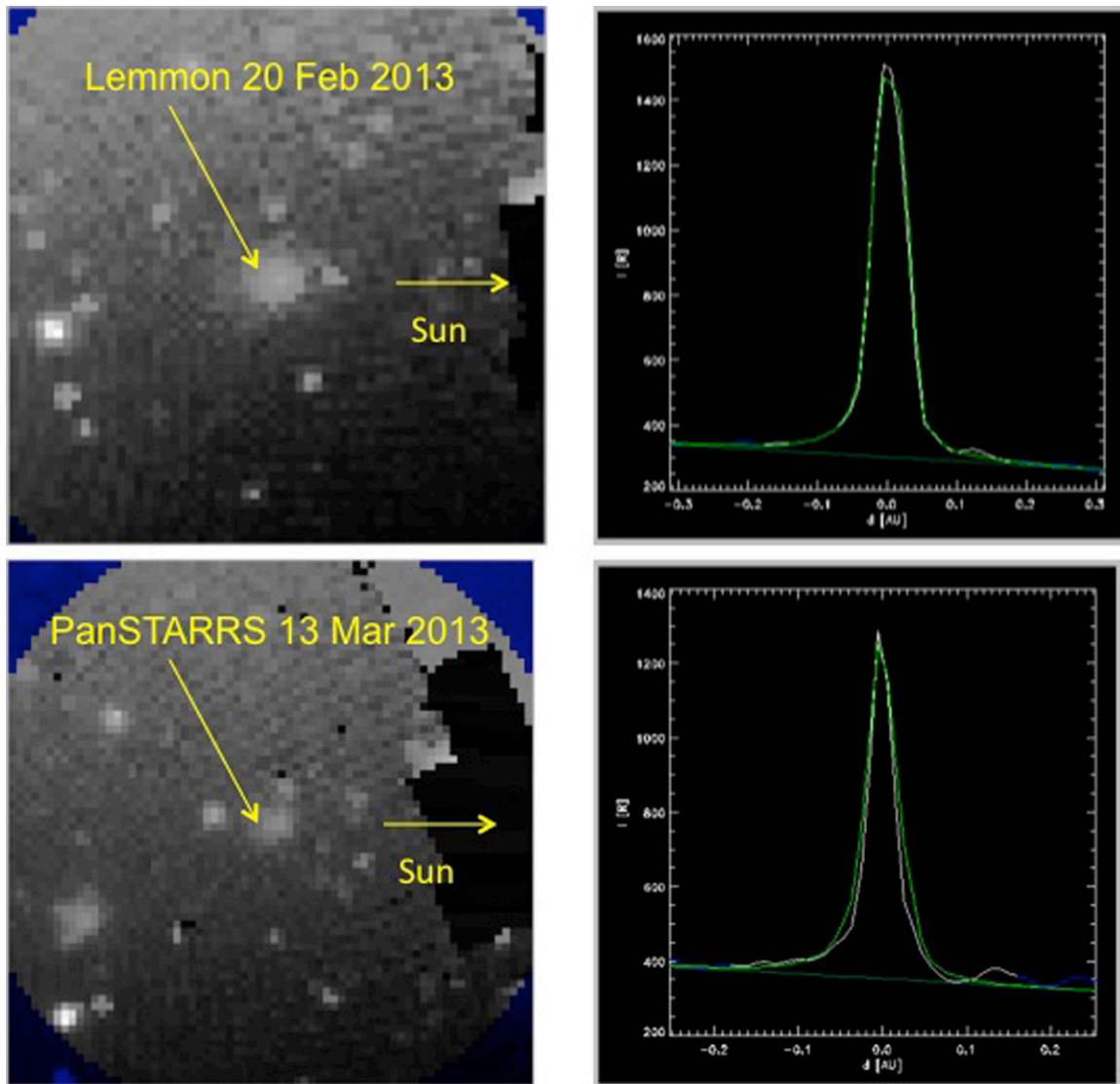


Figure 1. $\text{Ly}\alpha$ comae of C/2012 F6 (Lemmon) and C/2011 L4 (PanSTARRS). (a) On the left are $30^\circ \times 30^\circ$ renderings of the $\text{Ly}\alpha$ SWAN image of the comae of both comets extracted from the full-sky images on February 20 and March 13, respectively. It is a simple gray-scale representation that is nonlinear and stretched interactively to enhance features for visual inspection. The comet appears at the center of each image and is rotated so the Sun, as indicated, is toward the right. A number of field stars are apparent, as is the area around the Sun in the SWAN avoidance area. The plots on the right compare model data profiles along cuts through the images. The white curve is the observation. The green curve is the best-fit hydrogen coma model from which the water production rate is calculated for this day. The green straight line, tilted from lower left toward the upper right, is the fit to the local sky background from the interplanetary medium.

at heliocentric distances less than 2–3 AU. Of course, comets at smaller distances from *SOHO* (approximate geocentric distance) are more easily detected.

In this paper, we present large FOV ultraviolet observations of the hydrogen $\text{Ly}\alpha$ comae surrounding comets C/2011 L4 (PanSTARRS) and C/2012 F6 (Lemmon) made with the SWAN instrument on the *SOHO* spacecraft (Bertaux et al. 1997). An analysis of these observations yields total water production rates (50 for 2011 L4 and 109 for 2012 F6) covering many months of both comets' apparitions around their respective perihelia. These results are presented, compared with other observations, and discussed.

2. OBSERVATIONS AND ANALYSIS

Comet 2011 L4 PanSTARRS was observed in 50 full-sky SWAN images from 2013 January 29 through 2013 April 30. The comet reached a perihelion of 0.302 AU on 2013

March 10.17. Comet 2012 F6 (Lemmon) was observed in 109 full-sky SWAN images from 2012 November 29 through 2013 June 30. For both comets, this corresponds roughly to one useful image about every two days over the entire period, which is a typical yield for SWAN. Only single-image water production rates are presented here for understanding the time variation of water production. A water production rate is determined from each image using a model that accounts for the photochemical lifetimes, their heliocentric distance dependence, exothermic kinetics, and partial thermalization of hot H atoms (Mäkinen & Combi 2005). The model parameters have been determined by a series of more detailed model analyses of both images and high-resolution spectra of hydrogen observations of comets going back 25 yr (Combi et al. 2005). For these comets, the signal-to-noise ratio was unfortunately not large enough for our processing, which analyzes whole sequences of images simultaneously to determine daily-average values of the water production rate from the region around the nucleus (see, e.g.,

Table 1
SOHO/SWAN Observations of Comet 2011 L4 (PanSTARRS)
and Water Production Rates

ΔT (days)	r (AU)	Δ (AU)	g (s^{-1})	Q ($10^{28} s^{-1}$)	δQ ($10^{28} s^{-1}$)
-44.470	1.154	1.819	0.002062	13.97	0.73
-43.470	1.135	1.793	0.002061	14.74	0.71
-41.470	1.095	1.742	0.002084	12.32	0.54
-40.470	1.076	1.716	0.002083	16.82	0.27
-36.470	0.995	1.614	0.002103	25.80	0.25
-35.475	0.975	1.589	0.002102	15.83	0.34
-34.475	0.954	1.564	0.002101	10.55	0.47
-33.475	0.934	1.539	0.002100	11.63	0.31
-30.474	0.871	1.466	0.002121	12.08	0.36
-25.499	0.764	1.352	0.002138	11.88	0.33
-23.499	0.721	1.309	0.002137	14.64	0.84
-22.499	0.699	1.289	0.002136	20.38	0.42
-21.499	0.677	1.269	0.002156	18.19	0.30
-20.499	0.655	1.250	0.002156	24.01	0.26
-19.499	0.633	1.231	0.002155	21.26	0.28
-18.499	0.611	1.214	0.002154	28.72	0.25
-17.499	0.589	1.197	0.002153	22.89	0.28
-16.500	0.567	1.182	0.002152	26.31	0.31
-15.473	0.544	1.167	0.002151	27.30	0.26
-14.473	0.522	1.153	0.002129	30.65	0.30
-13.473	0.500	1.141	0.002128	31.49	0.27
-7.443	0.378	1.095	0.001958	32.52	0.35
-7.262	0.375	1.095	0.001958	37.37	0.34
-6.262	0.358	1.092	0.001883	63.40	0.35
-5.262	0.343	1.091	0.001814	55.01	0.38
-4.290	0.330	1.092	0.001754	93.58	0.39
-2.292	0.310	1.096	0.001621	87.63	0.55
8.726	0.402	1.167	0.001851	43.19	12.78
9.726	0.422	1.174	0.001869	30.20	2.51
10.728	0.442	1.182	0.001887	21.64	9.28
20.814	0.662	1.263	0.001937	14.79	3.56
21.814	0.684	1.271	0.001937	13.86	1.40
22.841	0.707	1.280	0.001916	14.98	0.17
27.504	0.808	1.318	0.001913	6.83	0.53
28.504	0.829	1.326	0.001893	4.66	0.53
29.502	0.850	1.334	0.001892	7.88	0.39
30.502	0.871	1.342	0.001892	8.19	0.35
31.502	0.892	1.351	0.001891	6.57	0.40
32.475	0.913	1.359	0.001890	6.25	0.46
33.475	0.934	1.367	0.001871	8.53	0.41
34.473	0.954	1.375	0.001870	7.94	0.44
35.474	0.975	1.384	0.001869	18.46	0.23
36.473	0.995	1.392	0.001869	5.26	0.73
43.417	1.134	1.450	0.001827	3.07	0.82
44.417	1.153	1.459	0.001826	1.61	1.61
45.417	1.173	1.468	0.001825	1.47	1.76
46.416	1.192	1.476	0.001825	9.02	0.27
48.416	1.230	1.494	0.001805	4.22	0.71
49.416	1.249	1.502	0.001805	1.54	1.77
51.389	1.286	1.520	0.001803	1.90	1.19

Notes. ΔT : time from perihelion on 2013 March 10.17 UT in days; r : heliocentric distance (AU); Δ : geocentric distance (AU); g : solar Ly α g factor (photons s^{-1}) at 1 AU; Q : water production rates for each image (s^{-1}); δQ : internal 1σ uncertainties.

Combi et al. 2005) using the extended spatial information in the large FOV SWAN images that translates into temporal information. This is enabled by the long lifetime of H atoms due to a combination of photoionization, charge exchange with solar protons, and impact by solar wind electrons (i.e., about 20 days at 1 AU).

Table 2
SOHO/SWAN Observations of Comet 2012 F6 (Lemmon)
and Water Production Rates

ΔT (days)	r (AU)	Δ (AU)	g (s^{-1})	Q ($10^{28} s^{-1}$)	δQ ($10^{28} s^{-1}$)
-105.443	1.979	2.018	0.001855	4.26	0.72
-94.413	1.826	1.728	0.001869	5.27	0.49
-93.413	1.813	1.703	0.001868	6.81	0.35
-92.413	1.799	1.677	0.001868	6.03	0.43
-91.413	1.785	1.652	0.001867	4.47	0.44
-90.398	1.770	1.627	0.001866	6.79	0.37
-85.385	1.700	1.505	0.001862	7.43	0.21
-66.955	1.439	1.133	0.001848	9.12	0.31
-58.014	1.312	1.023	0.001841	19.45	0.15
-56.026	1.284	1.007	0.001840	22.99	2.00
-53.043	1.242	0.989	0.001838	14.55	0.11
-51.043	1.215	0.981	0.001836	15.60	0.13
-50.053	1.201	0.978	0.001835	15.06	0.14
-49.053	1.187	0.976	0.001813	17.24	0.11
-48.053	1.173	0.975	0.001812	18.13	0.12
-46.053	1.146	0.976	0.001810	20.71	0.11
-40.046	1.065	0.996	0.001787	26.39	0.10
-39.046	1.052	1.002	0.001786	28.89	0.06
-37.022	1.026	1.016	0.001785	25.25	0.11
-36.021	1.013	1.024	0.001784	26.47	0.34
-35.021	1.000	1.033	0.001765	30.50	0.10
-28.990	0.927	1.093	0.001743	36.74	0.10
-27.990	0.915	1.105	0.001726	33.72	0.11
-26.963	0.904	1.117	0.001725	43.30	0.09
-25.963	0.893	1.129	0.001709	36.41	0.10
-24.961	0.882	1.141	0.001708	45.73	0.11
-21.934	0.851	1.180	0.001691	40.48	0.14
-20.934	0.841	1.193	0.001676	50.34	0.11
-19.932	0.832	1.206	0.001675	49.85	2.66
-18.932	0.823	1.219	0.001660	55.67	0.12
-17.906	0.814	1.233	0.001646	45.78	0.13
-16.906	0.805	1.247	0.001646	65.45	0.10
-15.906	0.797	1.260	0.001633	70.13	0.09
-14.904	0.789	1.274	0.001620	86.79	0.11
-13.904	0.782	1.287	0.001619	74.18	2.69
-12.877	0.775	1.301	0.001609	80.06	4.36
-10.877	0.763	1.328	0.001589	75.51	0.11
-9.874	0.758	1.341	0.001589	67.87	6.36
-7.874	0.748	1.367	0.001572	73.92	0.12
-6.848	0.744	1.380	0.001565	73.53	0.16
-5.848	0.741	1.392	0.001558	74.54	0.12
-4.846	0.738	1.404	0.001551	79.23	0.09
-3.846	0.735	1.417	0.001546	78.28	0.13
-2.846	0.733	1.428	0.001541	95.86	0.11
-1.819	0.732	1.440	0.001536	101.80	0.11
0.181	0.731	1.463	0.001533	119.70	0.10
1.183	0.732	1.474	0.001530	112.50	0.11
3.183	0.734	1.494	0.001527	97.50	0.14
4.209	0.736	1.505	0.001526	90.62	0.12
5.209	0.739	1.514	0.001525	106.40	0.09
8.213	0.750	1.542	0.001527	88.69	0.12
9.443	0.755	1.552	0.001529	90.06	0.10
10.443	0.761	1.560	0.001532	69.92	0.09
11.443	0.766	1.568	0.001537	87.79	0.08
12.440	0.772	1.576	0.001543	75.90	0.07
13.440	0.779	1.583	0.001543	84.65	0.09
14.440	0.786	1.590	0.001549	81.72	0.11
15.440	0.794	1.596	0.001558	95.31	0.11
16.414	0.801	1.603	0.001557	74.16	0.11
17.415	0.809	1.609	0.001566	80.00	0.10
18.414	0.818	1.615	0.001575	91.38	0.09
19.414	0.827	1.620	0.001574	103.90	0.07
21.357	0.845	1.631	0.001583	94.12	0.06
22.357	0.855	1.636	0.001593	111.00	0.07

Table 2
(Continued)

ΔT (days)	r (AU)	Δ (AU)	g (s^{-1})	Q ($10^{28} s^{-1}$)	δQ ($10^{28} s^{-1}$)
23.357	0.865	1.640	0.001592	95.15	0.06
25.358	0.886	1.649	0.001602	73.24	0.06
26.358	0.897	1.653	0.001613	69.38	0.08
28.357	0.920	1.661	0.001612	55.54	0.09
29.358	0.931	1.664	0.001623	54.61	0.07
30.357	0.943	1.668	0.001622	47.91	0.08
31.375	0.955	1.671	0.001622	49.49	0.08
32.375	0.967	1.674	0.001635	37.14	0.08
33.375	0.980	1.677	0.001634	44.05	0.07
34.375	0.992	1.679	0.001633	41.02	0.09
35.378	1.005	1.682	0.001633	37.25	0.08
36.378	1.017	1.684	0.001646	43.22	0.07
38.395	1.043	1.689	0.001645	42.00	0.08
39.395	1.056	1.692	0.001644	40.51	0.08
40.395	1.070	1.694	0.001643	37.99	1.36
41.395	1.083	1.695	0.001657	45.31	1.02
42.398	1.096	1.697	0.001656	29.23	0.20
43.398	1.110	1.699	0.001655	29.54	0.15
51.427	1.220	1.711	0.001665	32.91	0.15
52.450	1.234	1.712	0.001665	29.06	2.01
53.449	1.248	1.713	0.001664	28.96	0.15
54.449	1.262	1.715	0.001664	32.71	0.14
55.449	1.276	1.716	0.001663	25.55	0.26
56.457	1.290	1.717	0.001663	19.65	0.95
57.457	1.304	1.718	0.001662	21.94	0.20
58.457	1.319	1.719	0.001661	23.49	0.18
59.478	1.333	1.721	0.001661	19.91	0.21
60.478	1.347	1.722	0.001660	22.98	0.22
61.478	1.361	1.723	0.001660	23.11	1.23
62.486	1.376	1.724	0.001659	19.81	0.22
64.486	1.404	1.727	0.001658	17.68	0.26
72.515	1.518	1.739	0.001653	17.03	0.24
73.535	1.533	1.741	0.001652	20.33	0.17
74.535	1.547	1.743	0.001652	20.93	0.20
75.535	1.561	1.745	0.001651	16.41	0.22
76.544	1.575	1.747	0.001651	15.86	0.23
77.544	1.589	1.749	0.001650	17.83	0.22
78.544	1.604	1.751	0.001649	17.17	0.21
79.564	1.618	1.754	0.001649	18.01	0.23
80.564	1.632	1.756	0.001648	17.77	0.47
86.592	1.717	1.773	0.001645	18.76	1.04
87.592	1.731	1.776	0.001644	17.67	0.19
89.592	1.759	1.783	0.001643	19.24	0.87
90.592	1.773	1.786	0.001643	13.78	0.47
99.409	1.896	1.823	0.001624	14.10	0.21

Notes. ΔT : time from perihelion on 24.51 March 2013 UT in days; r : heliocentric distance (AU); Δ : geocentric distance (AU); g : solar Ly α g factor (photons s^{-1}) at 1 AU; Q : water production rates for each image (s^{-1}); δQ : internal 1σ uncertainties.

The Ly α fluorescence rate (g factor) was determined using the daily composite solar Ly α data taken from the LASP, University of Colorado Web site <http://lasp.colorado.edu/lisird/lya> and the Ly α line profile (Lemaire et al. 1998) to get the variation of the g factor with heliocentric velocity in the standard manner. The SWAN calibration at Ly α has been recently revised using a comparison with the *Hubble Space Telescope* Goddard High Resolution Spectrograph measurements of the IPM (Qu  merais et al. 2009; Clarke et al. 1998). Combi et al. (2011) described the effect of the recalibration on comet observations over the time since the first SWAN measurements of C/1996 B2 (Hyakutake). Table 1 gives the observational circumstances, average g factors,

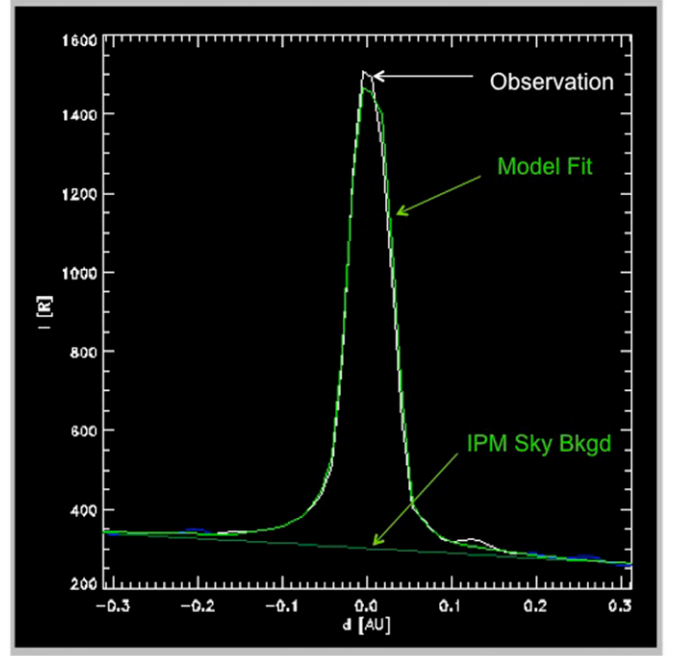


Figure 2. Model analysis of a Ly α image of comet C/2012 F6 (Lemmon). A plot of brightness in Rayleighs vs. distance from the comet in astronomical units is shown. The white profile corresponds to the measurement, the green profile to the model fit, and the lower green straight line to the model fit to the nearby interplanetary hydrogen background.

production rates, and their formal uncertainties for all images of comet C/2011 L4 (PanSTARRS). Table 2 gives the same information for C/2012 F6 (Lemmon).

Examples of the Ly α images and the resulting model fits from the analysis are shown in Figure 1. To the left, the 30 deg² field subsets of the full-sky SWAN images of both comets are rendered with the comet at the center and the Sun to the right, surrounded by field stars. To the right, the profile slices through each image show the main components of the image, the comet and interplanetary Ly α medium (IPM) background, and how they are reproduced by the detailed model analysis procedure. The white curved lines show the observed intensity profiles through the comet, the similar green curves give the fitted model profiles, and, finally, the green straight lines show the model fits to the background IPM signal from interstellar hydrogen streaming through the solar system. The production rates are determined by the model fit to the entire two-dimensional image, typically within a circular aperture of a 5 $^\circ$ radius, and not just this or any single profile.

A larger version of the model/data comparison is shown in Figure 2 for comet C/2012 F6 (Lemmon) only. The original pixels from the full-sky SWAN images are resorted into a small image with the comet centered and the Sun to the right, as shown in Figure 1. Most of the discrete features in the image are field stars. By comparing images from one night to the next, we can identify the field stars and eliminate any contribution they might make to our analysis. Interference with field stars is the main reason why we have a typical yield of usable images on about half the days. The galactic equator is naturally the most problematic region.

Another approach is to subtract two images from different days, which minimizes the influence of most field stars. Although the spatial registration on two different full-sky images is not perfect, and so the resulting subtraction is not

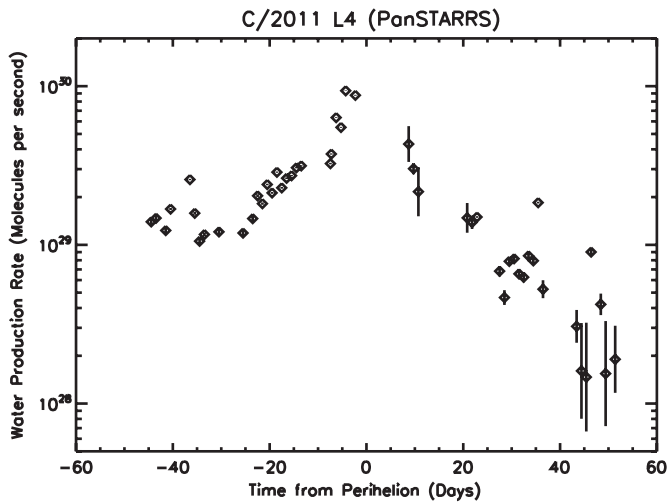


Figure 3. Water production rate of Comet C/2011 L4 (PanSTARRS) plotted as a function of time in days from perihelion on 2013 March 10.17. The diamonds give the values from the SWAN observations. The error bars correspond to internal 1σ uncertainties from photon counts and background subtraction. Systematic uncertainties from model assumptions and calibration are of the order of 30%.

perfect on a single-pixel level, averaging the result over the typical 5° – 8° radius circular area is effective in averaging out the spatial registration errors. The potential contribution of faint background stars near or below the obvious detection limit is probably responsible for some of the day-to-day variations in the determined production rates that appear to be above three times the 1σ error bars shown in the figures and tables, as was already discussed in the model description paper (Mäkinen & Combi 2005). These stars could contribute to overestimate either the coma or the IPM background and should not result in a systematic error.

Figure 3 shows the water production rate for comet C/2011 L4 (PanSTARRS), determined by modeling each individual image plotted versus time in days from perihelion on 2013 March 10.17. The internal 1σ stochastic uncertainties from

photon counts and background subtraction are indicated by the error bars on each point. In addition to these random uncertainties, calibration and various model assumptions and parameters contribute to potential systematic uncertainties on the order of 30%. There is a large and noteworthy asymmetry of the variation of the water production rate with respect to perihelion.

The asymmetry in the water production rate about perihelion is also seen in the visual light curve (Yoshida, <http://www.aerith.net/comet/catalog/index-T-earth.html>). At about 36 days before perihelion (February 12), a small outburst peaked that lasted between 6 and 7 days in total. The peak of the outburst was about a factor of two higher ($2.6 \times 10^{29} \text{ s}^{-1}$) than the baseline level just before and after ($1.2 \times 10^{29} \text{ s}^{-1}$). The total excess water mass released during this outburst was $1.1 \times 10^9 \text{ kg}$. This outburst was only about 20% of the noted outburst of comet 1996 B2 (Hyakutake) on 1996 March 19 (Bertaux et al. 1998; Combi et al. 2005), which was accompanied by a major fragmentation of the nucleus (Harris et al. 1997). The durations of the outbursts in the two comets were similar and occurred at similar heliocentric distances. This could be interpreted as a release of a similar size distribution of particles that sublimated over a similar length of time temporarily raising the production rate of the comet. There were other peaks that are only single point values and therefore are less reliable as an indicator of a real outburst.

The water production rate is plotted as a function of heliocentric distance in Figure 4. This format accentuates the different behavior pre- and post-perihelion. The power-law fits are $Q = 1.3 \times 10^{29} r^{-1.3} \text{ in s}^{-1}$ and $Q = 5.0 \times 10^{28} r^{-2.3} \text{ in s}^{-1}$ for the pre-perihelion and post-perihelion periods, respectively, where r is the heliocentric distance. Such behavior, with a fairly shallow slope before perihelion and a steeper slope after perihelion, is often seen in new comets coming on their first trip back into the inner solar system directly from the Oort Cloud since they were formed 4.5 Gyr ago and ejected into the Oort Cloud by the giant planets (A’Hearn et al. 1995; Combi et al. 2008, 2009). The behavior of 2011 L4 (PanSTARRS) is actually quite

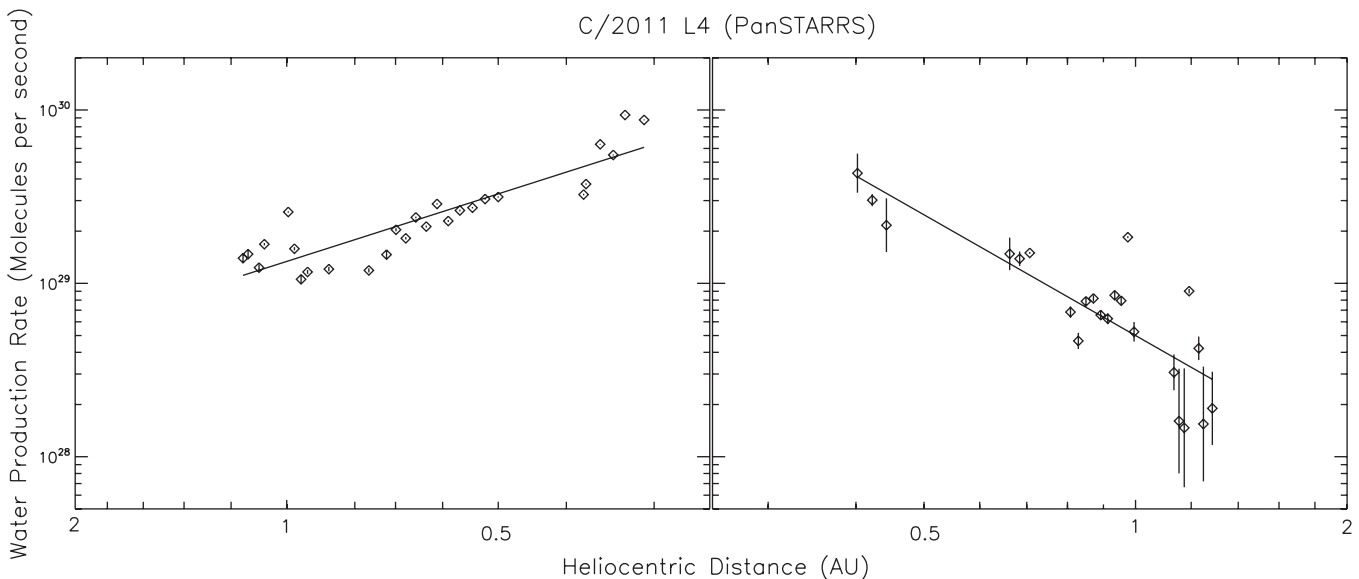


Figure 4. Water production rates of Comet 2011 L4 (PanSTARRS) plotted as a function of heliocentric distance in AU. The diamonds are the values from the SWAN observations. The error bars correspond to internal 1σ uncertainties from photon counts and background subtraction. Systematic uncertainties from model assumptions and calibration are of the order of 30%. The lines are power-law fits to the pre- and post-perihelion data separately, giving the water production rates of $1.3 \times 10^{29} r^{-1.3} \text{ s}^{-1}$ and $5.0 \times 10^{28} r^{-2.3} \text{ s}^{-1}$, for each, respectively.

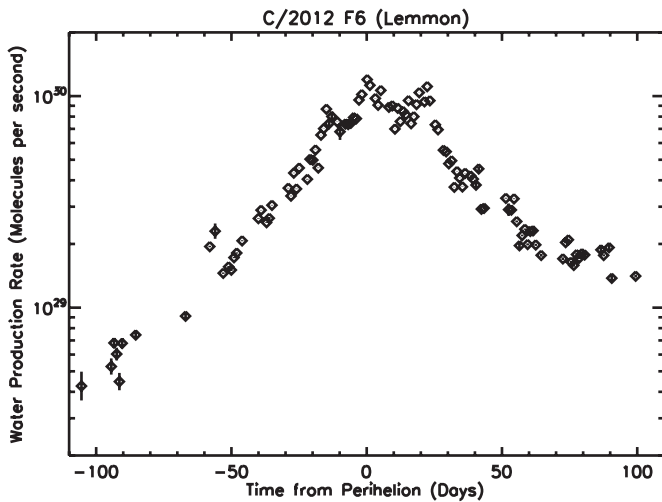


Figure 5. Water production rates of Comet C/2012 F6 (Lemmon) plotted as a function of time in days from perihelion on 2013 March 24.51. The diamonds give the values from the SWAN observations. The error bars correspond to internal 1σ uncertainties from photon counts and background subtraction. Systematic uncertainties from model assumptions and calibration are of the order of 30%.

reminiscent of another Oort Cloud comet, 2002 T7 (LINEAR), as shown by Combi et al. (2009).

Figure 5 shows the water production rate of comet C/2012 F6 (Lemmon) plotted as a function of time in days from perihelion on 2013 March 24.51. Its variation is also asymmetric about perihelion, but with generally lower activity before perihelion compared to after. There is some interesting variation of water production around perihelion with three small peaks in activity: 20 days before perihelion, at perihelion, and 22 days after perihelion. The visual light curve (Yoshida, <http://www.aerith.net/comet/catalog/index-T-earth.html>) of the comet does not show this irregular activity; however, the coverage of the visual light curve within the month centered around perihelion is fairly sparse. On the other hand, the overall shape of the variation showing the generally lower levels in the months

before perihelion compared with after perihelion are clearly present in both the water production rates and the visual light curve.

Figure 6 shows both the water production rate before and after perihelion plotted as a function of heliocentric distance. A typical comet whose activity is controlled by some average active surface area (e.g., the nucleus) will have a production rate that varies with heliocentric distance, r , for $r < 2$ AU with a power law between r^{-2} and r^{-3} . When a comet has either a very elongated shape and/or a very non-uniform distribution of active regions on the surface, then strong deviations from this behavior are possible due to seasonal effects as the orientations of these active regions with respect to the nucleus spin axis and with respect to solar illumination change as the comet orbits. Clearly, sporadic activity of the nucleus itself could also affect its behavior over the orbit. The lines in Figure 6 show the best-fit power laws to the pre- and post-perihelion data such that the water production rates can be expressed as $3.2 \times 10^{29} r^{-3.0} \text{ s}^{-1}$ and $4.8 \times 10^{29} r^{-2.3} \text{ s}^{-1}$, respectively.

3. SUMMARY

Here, we show results of a determination of water production in comets C/2011 L4 (PanSTARRS) and C/2012 F6 (Lemmon) throughout their apparitions in the first half of 2013. The results were extracted from an analysis of the observations made with the SWAN instrument on the *SOHO* spacecraft of the atomic hydrogen coma seen in emission at $\text{Ly}\alpha$. As with the many comets already observed with *SOHO*/SWAN, the variations of water production rates of both comets are clearly consistent with their different stages of evolution.

The very shallow slope of the inbound pre-perihelion leg of the apparition of comet C/2011 L4 (PanSTARRS), combined with its more normal outbound $r^{-2.3}$ variation, is fully consistent with this comet being an Oort Cloud comet on its first passage into the inner solar system since it was placed there 4.5 Gyr ago. In this regard, the activity is also consistent with its eccentricity. The shallow pre-perihelion slope in the best-fit power-law variation is not uncommon in new Oort Cloud comets

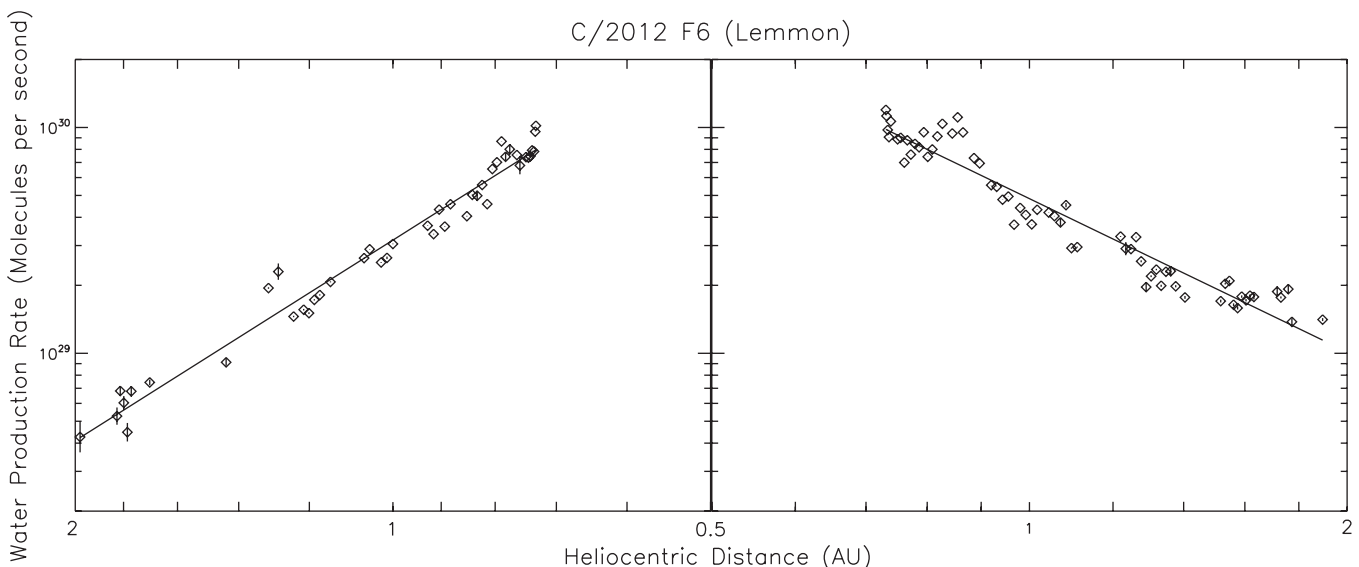


Figure 6. Water production rates of Comet 2012 F6 (Lemmon) plotted as a function of heliocentric distance in AU. The diamonds are the values from the SWAN observations. The error bars correspond to internal 1σ uncertainties from photon counts and background subtraction. Systematic uncertainties from model assumptions and calibration are of the order of 30%. The lines are power-law fits to the pre- and post-perihelion data separately, giving water production rates of $3.2 \times 10^{29} r^{-3.0} \text{ s}^{-1}$ and $4.8 \times 10^{29} r^{-2.3} \text{ s}^{-1}$, for each, respectively.

(e.g., Combi et al. 2009). The limited available water production rates with which we can compare are somewhat lower (Paganini et al. 2013) than our value, but are within the typical range of relative agreement among different determinations of water production rates in comets. They do not differ enough to be deemed inconsistent. There was one small outburst seen at 36 days before perihelion on February 12.

Comet C/2012 F6 (Lemmon), on the other hand, behaved similarly on inbound and outbound legs of its orbit with moderate asymmetry in the opposite sense as 2011 L4 (PanSTARRs). This, combined with its lower eccentricity indicating a semi-major axis of ~ 490 AU, is fully consistent with this being a long-period Oort Cloud comet that has been to the inner solar system on previous orbits and might be expected to return in another $\sim 10^4$ yr. Lemmon had three small outbursts around perihelion: 20 days before perihelion, at perihelion, and 22 days after perihelion. These were all smaller in magnitude than the one by comet C/2011 L4 (PanSTARRs).

SOHO is an international cooperative mission between ESA and NASA. M.C. acknowledges support from grant NNX11AH50G from the Planetary Astronomy Program. J.T.T.M. was supported by the Finnish Meteorological Institute (FMI). J.-L.B. and E.Q. acknowledge support from CNRS and CNES. We obtained cometary ephemerides and orbital elements from the JPL Horizons Web site (<http://ssd.jpl.nasa.gov/horizons.cgi>). The composite solar Ly α data was taken from the LASP Web site of the University of

Colorado (<http://lasp.colorado.edu/lisird/lya/>). We acknowledge the personnel that have been keeping *SOHO* and SWAN healthy and operational for over 18 yr, particularly Walter Schmidt at FMI. We also thank Dr. Lucas Paganini for discussions regarding his observations of C/2011 L4 (PanSTARRs) before publication.

REFERENCES

- A'Hearn, M. F., Millis, R. L., Schleicher, D. G., Osip, D. J., & Birch, P. V. 1995, *Icar*, **118**, 223
- Bertaux, J. L., Combi, M. R., Qu  merais, E., & Schmidt, W. 2014, *P&SS*, **91**, 14
- Bertaux, J. L., Costa, J., Qu  merais, E., et al. 1998, *P&SS*, **46**, 555
- Bertaux, J. L., Qu  merais, E., Lallement, R., et al. 1997, *SoPh*, **175**, 737
- Clarke, J. T., Lallement, R., Bertaux, J.-L., et al. 1998, *ApJ*, **499**, 482
- Combi, M. R., Lee, Y., Patel, T. S., et al. 2011, *AJ*, **141**, 128
- Combi, M. R., M  kinen, J. T. T., Bertaux, J.-L., Lee, Y., & Qu  merais, E. 2009, *AJ*, **137**, 4734
- Combi, M. R., M  kinen, J. T. T., Bertaux, J.-L., & Qu  merais, E. 2005, *Icar*, **177**, 228
- Combi, M. R., M  kinen, J. T. T., Henry, N. J., Bertaux, J.-L., & Qu  merais, E. 2008, *AJ*, **135**, 1533
- Gibbs, A. R. 2012, *CBET*, **3133**, 1
- Harris, W. M., Combi, M. R., Honeycutt, R. K., & Mueller, B. E. A. 1997, *Sci*, **277**, 676
- Lemaire, P., Emerich, C., Curdt, W., Schuehle, U., & Wilhelm, K. 1998, *A&A*, **334**, 1095
- M  kinen, J. T. T., & Combi, M. R. 2005, *Icar*, **177**, 217
- Paganini, L., Mumma, M. J., Villanueva, G. L., et al. 2013, *IAUC*, **9255**, 1
- Qu  merais, E., Lallement, R., Sandel, B. R., & Clarke, J. 2009, *SSRv*, **143**, 151
- Wainscoat, R., Micheli, M., Wells, L., et al. 2011, *IAUC*, **9215**, 1